Numerical Simulations of Hall MHD Turbulence with Magnetization*)

Hideaki MIURA and Fujihiro HAMBA[1)]

National Institute for Fusion Science, 322-6 Oroshi-cho, Toki, Gifu 509-5292, Japan
[1)]*Institute of Industrial Science, the University of Tokyo, 4-6-1 Komaba, Meguro-ku, Tokyo 153-8505, Japan*

(Received 6 January 2023 / Accepted 20 February 2023)

Direct numerical simulations (DNS) and large eddy simulations (LES) of homogeneous Hall magnetohydrodynamic (MHD) simulations are carried out to verify the properties of a sub-grid-scale (SGS) model which has been developed for LES recently. LES with the new SGS model reproduces one-dimensional spectra of DNS. It is also shown that the probability density functions (PDFs) of the current density components of DNS and LES in the grid-scale coincide with each other by an appropriate normalization. We verify by this numerical study that our improved SGS model is applicable to homogeneous Hall MHD turbulence. We also find that the difference in the deviation of the current density components is smaller in the MHD-scale of LES than in that of DNS. These results provide a new insight to study the spectral anisotropy of turbulence, especially in relation to the sub-ion-scale.

Keywords: Hall MHD turbulence, uniform magnetic field, SGS model, verification

DOI: 10.1585/pfr.18.2401022

1. Introduction

MHD turbulence has been studied extensively over decades to clarify its ubiquitous and universal nature such as the inertial sub-range power-law in the energy spectrum, and various physical mechanisms which sustain the natures [1–3]. More recently, another power-law in the sub-ion-scale has gathered attention as well, and has been studied by the Hall MHD model [4–10].

In numerical simulations of Hall MHD turbulence (or an extended MHD simulation of torus plasma which keeps the Hall term in the system of equations as well), providing a wide range of the wave-numbers both for the MHD-scale and the sub-ion-scales is not very easy. In order to ease the difficulty, we consider low-pass filtering the Hall MHD equations, and solve the low-pass filtered (grid-scale, GS) equations. This allows us to keep the influence of the sub-ion-scale to the MHD-scale and provide a wider wave-number range for the MHD-scale. For this technique, LES, we need to replace some terms which originate from the filtering of the nonlinear terms and represent influences of high wave-number components to low wave-number (GS) components by a phenomenological model, a sub-grid-scale (SGS) model.

We have developed our first SGS model for the Hall MHD equations both with and without background constant magnetic field [11], and applied the SGS model for LES of nonlinear growth of ballooning modes in the Large Helical Device (LHD), a nuclear fusion experiment facility [12]. Then the model has been improved so that the SGS model can give a higher effective resolution for homogeneous and isotropic turbulence [13]. Since the new model is not verified for anisotropic turbulence, we verify the applicability of the improved SGS model for a forced homogeneous turbulence under the mean magnetic field, and provide a perspective to apply the model to our applications of magnetized plasmas.

This paper is organized as follows. In §2, the GS Hall MHD equations and the SGS model are introduced. In §3, numerical results are presented. Finally in §4, concluding remarks are presented.

2. Hall MHD Equations and SGS Model

Incompressible Hall MHD equations can be expressed as

$$\frac{\partial u_i}{\partial t} = -\frac{\partial}{\partial x_j}\left[\left(u_i u_j - B_i B_j\right) + \left(p + \frac{1}{2}B_k B_k\right)\delta_{ij}\right] + \nu\frac{\partial S_{ij}}{\partial x_j} + f_i, \tag{1}$$

$$S_{ij} = \frac{\partial u_i}{\partial x_j} + \frac{\partial u_j}{\partial x_i}, \tag{2}$$

$$\frac{\partial B_i}{\partial t} = -\epsilon_{ijk}\frac{\partial E_k}{\partial x_j}, \tag{3}$$

$$E_i = -\epsilon_{ijk}\left(u_j - \epsilon_H J_j\right)B_k + \eta J_i, \tag{4}$$

with the incompressible (solenoidal) conditions $\partial u_k/\partial x_k = \partial B_k/\partial x_k = 0$. The three symbols with one index B_i, $J_i = \epsilon_{ijk}\partial_j B_k$, and u_i represent the i-th components of the

author's e-mail: miura.hideaki@nifs.ac.jp

*) This article is based on the presentation at the 31st International Toki Conference on Plasma and Fusion Research (ITC31).

magnetic field, the current density, and velocity field vectors, respectively. Tensor symbols δ_{ij} and ϵ_{ijk} are the Kronecker's delta and the Levi-Civita's anti-symmetric tensor, respectively. The sum of 1, 2, and 3 is taken for repeated suffixes of the vector and tensor variables. See Ref. [13] for the normalization of the equations. The symbols ϵ_H, η, and ν are the Hall parameter (the ratio of the ion skin depth to the system length), magnetic diffusivity, and shear viscosity, respectively. Since the equations have been normalized, $1/\nu$ and $1/\eta$ can be understood as the reference Reynolds number and the Lundquist number, respectively.

The equations (1)-(4) are operated by a low-pass filter of a filter width Δ to obtain the GS Hall MHD equations as

$$\frac{\partial \overline{u}_i}{\partial t} = -\frac{\partial}{\partial x_j}\left[\left(\overline{u}_i\overline{u}_j - \overline{B}_i\overline{B}_j\right) + \left(\overline{p} + \frac{1}{2}\overline{B}_k\overline{B}_k\right)\delta_{ij}\right] + \nu\frac{\partial \overline{S}_{ij}}{\partial x_j} - \frac{\partial \overline{\tau}_{ij}}{\partial x_j} + \overline{f}_i, \tag{5}$$

$$\overline{\tau}_{ij} = \left[\left(\overline{u_iu_j} - \overline{B_iB_j}\right) + \frac{1}{2}\overline{B_kB_k}\delta_{ij}\right] - \left[\left(\overline{u}_i\overline{u}_j - \overline{B}_i\overline{B}_j\right) + \frac{1}{2}\overline{B}_k\overline{B}_k\delta_{ij}\right], \tag{6}$$

$$\overline{S}_{ij} = \frac{\partial \overline{u}_i}{\partial x_j} + \frac{\partial \overline{u}_j}{\partial x_i}, \tag{7}$$

$$\frac{\partial \overline{B}_i}{\partial t} = -\epsilon_{ijk}\frac{\partial \overline{E}_k}{\partial x_j}, \tag{8}$$

$$\overline{E}_i = -\epsilon_{ijk}\left(\overline{u}_j - \epsilon_H\overline{J}_j\right)\overline{B}_k + \eta\overline{J}_i - \overline{E}_i^M - \overline{E}_i^H, \tag{9}$$

$$\overline{E}_i^M = \epsilon_{ijk}\left(\overline{u_jB_k} - \overline{u}_j\overline{B}_k\right), \tag{10}$$

$$\overline{E}_i^H = \epsilon_H\epsilon_{ijk}\left(-\overline{J_jB_k} + \overline{J}_j\overline{B}_k\right), \tag{11}$$

with the incompressible (solenoidal) conditions $\partial\overline{u}_k/\partial x_k = \partial\overline{B}_k/\partial x_k = 0$. Then the SGS model presented in Ref. [13] is introduced as

$$\overline{\tau}_{ij} = -\nu_{SGS}\overline{S}_{ij}, \tag{12}$$

$$\overline{E}_i^M + \overline{E}_i^H = -\eta_{SGS}\overline{J}_i + \epsilon_H\frac{\partial}{\partial x_j}\left(\nu_{SGS}\sigma_{H,1}\overline{S}_{ij}\right) - \epsilon_H^2\frac{\partial}{\partial x_j}\left[\nu_{SGS}\sigma_{H,2}\left(\frac{\partial \overline{J}_i}{\partial x_j} + \frac{\partial \overline{J}_j}{\partial x_i}\right)\right], \tag{13}$$

$$\nu_{SGS} = C_\nu\Delta^2\left(\frac{1}{2}C_\nu\overline{S}_{ij}^2 + C_\eta\overline{J}_i^2\right)^{1/2}, \tag{14}$$

$$\eta_{SGS} = C_\eta\Delta^2\left(\frac{1}{2}C_\nu\overline{S}_{ij}^2 + C_\eta\overline{J}_i^2\right)^{1/2}. \tag{15}$$

In the SGS model (12) - (15), the filter width Δ is usually given as $\Delta = \Delta_0 = (\Delta x_1\Delta x_2\Delta x_3)^{1/3}$. Giving a larger Δ corresponds to denoting a larger C_ν and C_η for $\Delta = \Delta_0$ as we have discussed in Ref. [13]. In this paper, two computations $\Delta = \Delta_0$ and $\Delta = 2\Delta_0$ are provided, as we see in the next section. Hereafter, we omit the symbol $\overline{\ }$ from a physical variable. All the physical variables below are those in the GS.

3. Numerical Results

Numerical simulations are carried out for one DNS and two LES (LES-H, LES-L). In DNS, eqs. (1) - (4) are solved numerically by the pseudo-spectral method and Runge-Kutta-Gill technique. Three-dimensional Fourier transform libraries P3DFFT [14] and FFTE [15] are used for the pseudo-spectral computations. The system size of the simulation is $L_1 = L_2 = 2\pi$ in x_1 and x_2 directions, respectively, and $L_3 = 16\pi$ in the x_3 direction. The number of grid points N_i in the x_i ($i = 1, 2, 3$) are given so that the grid width is the same in all three directions. Aliasing errors in the pseudo-spectral computations are removed by the 2/3-truncation method in each direction. Thus the numerical resolution is represented by the maximum wavenumber $k_{max} = 170$. The external force $\bar{f}_i$ in the velocity equations is given with fixed amplitudes and random phase in the Fourier space for $k = \sqrt{k_1^2 + k_2^2 + k_3^2} \leq 3$. Since the external random force stirs a large-scale fluid motion, we focus on the spectral shape and other statistical properties of $k \gg 3$.

In LES, eqs. (5) - (15) are solved by the same schemes as DNS. Parameters in (5) - (15) are presented in Table 1. In LES-H, the control parameters of the SGS are given as that provided by the original theory [16, 17]. This parameter set gives the effective numerical resolution $k_{eff} = 1/\Delta$, the same as the maximum resolution of the pseudo-spectral method k_{max}. In LES-L, the parameters are given so that $k_{eff} = 1/\Delta = k_{max}/2$. Although this parameter set provides smaller k_{eff} than LES-H, the effective resolution is twice as high as that utilized for the first time for the Hall MHD model [11], and gives a reasonable balance between the spectral resolution and representation in real space.

In the simulations, the third component of the magnetic field B_3, the mean magnetic field $B_0 = 1$ is added. Thus turbulence in our simulations is anisotropic. The turbulence energy and the mean magnetic energy are comparable to each other. In this sense the anisotropy is weak in this turbulence simulation study, being similar to the anisotropic turbulence reported in Ref. [11]. This weak-

Table 1 Parameters for DNS and LES of Hall MHD turbulence.

	DNS	LES-H	LES-L
N_1, N_2	512	128	128
N_3	4096	1024	1024
k_{max}	170	41	41
k_{eff}	-	41	20
ν	2×10^{-3}	2×10^{-3}	2×10^{-3}
η	2×10^{-3}	2×10^{-3}	2×10^{-3}
ϵ_H	0.05	0.05	0.05
C_ν	-	0.046	0.092
C_η	-	0.0329	0.0657
$\sigma_{H,1}$	-	1	8
$\sigma_{H,2}$	-	1	8

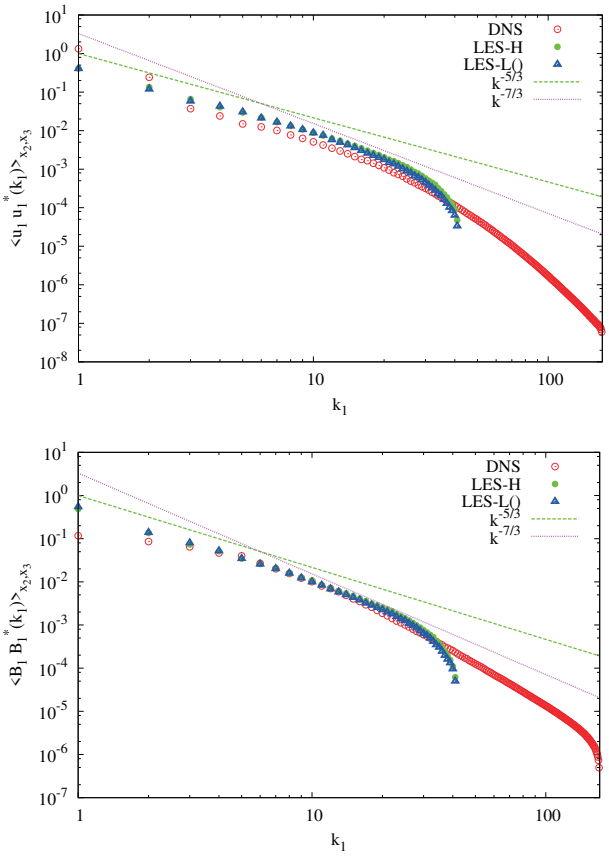

Fig. 1 One-dimensional spectra $E_{u_1u_1}(k_1)$ and $E_{B_1B_1}(k_1)$.

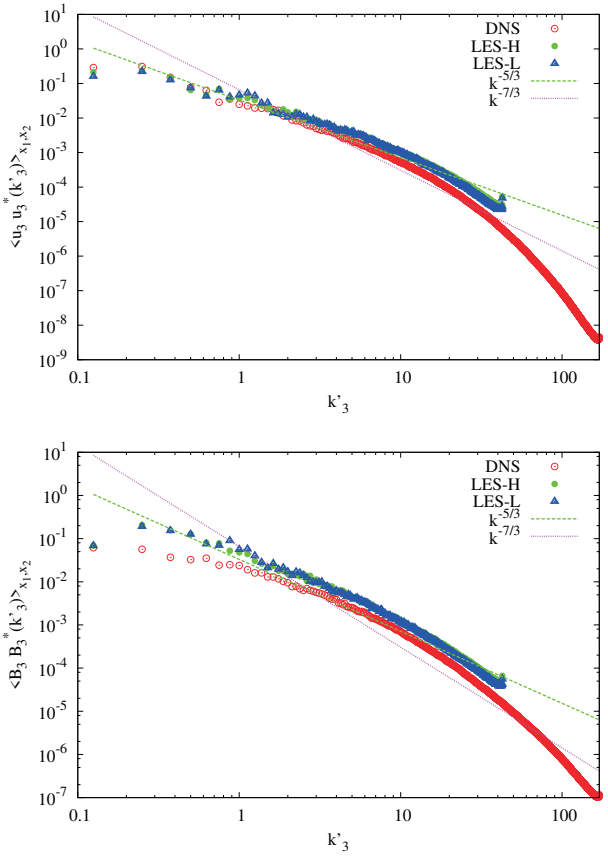

Fig. 2 One-dimensional spectra $E_{u_3u_3}(k_3')$ and $E_{B_3B_3}(k_3')$.

ness of the magnetization enables us to study the effectiveness of our SGS model which has been developed for isotropic turbulence to anisotropic turbulence. The Hall parameter ϵ_H is set 0.05 throughout this paper. This means that the wave-number range $k > 1/\epsilon_H = 20$ is the sub-ion-scale. The LES-H run resolves the sub-ion-scale ($k > 20$) as the GS, while the LES-L treats the wave-number range for dumping the MHD-scale information.

In Fig. 1, the one-dimensional spectra (a) $\left\langle \widetilde{u}_1 \widetilde{u}_1^* \right\rangle_{x_2,x_3}$ and (b) $\left\langle \widetilde{B}_1 \widetilde{B}_1^* \right\rangle_{x_2,x_3}$ are presented as the function of the wave-number k_1, where $\langle\cdot\rangle_{x_a,x_b}$ is the average on the $x_a - x_b$ plane and * represents the complex conjugate. Since the mean magnetic field is imposed on the third component B_3, this figure represents the perpendicular spectrum of the perpendicular vector components. (The words parallel and perpendicular are used for the direction of the mean magnetic field in the x_3 direction all through this paper.) We find that both of the two LES give a reasonable reproduction of the GS parts of DNS.

In Fig. 2, the one-dimensional spectra (a) $\left\langle \widetilde{u}_3 \widetilde{u}_3^* \right\rangle_{x_1,x_2}$ and (b) $\left\langle \widetilde{B}_3 \widetilde{B}_3^* \right\rangle_{x_1,x_2}$ are presented as a function of the wave-number k_3', where $k_3' = \frac{2\pi}{L} k_3$ is the wavenumber normalized by the system length L. Thus this figure represents the parallel spectrum of the parallel vector components. The parallel spectrum of the velocity by two LES presented in Fig. 2 (a) shows a reasonable agreement with that of DNS. Although the parallel magnetic energy spectrum $\left\langle \widetilde{B}_3 \widetilde{B}_3^* \right\rangle_{x_1,x_3}$ in Fig. 2 (b) in the two LES has a larger amplitude than that of DNS, the spectral profile is similar to each other. We come to this difference in amplitude later in the last section.

Next, we see the probability density function (PDF) of the current density components $J_i = \epsilon_{ijk}\partial_j B_k$ in Fig. 3. In order to see a difference among scales, we provide band-pass filters extracting three ranges, $10 < k' \leq 20$ (range I), $20 < k' \leq 40$ (range II), and $40 < k' \leq 80$ (range III), where $k' = \sqrt{k_1^2 + k_2^2 + k_3'^2}$. The range I is a part of the MHD-scale ($k' < 1/\epsilon_H$) excluding the low wave-numbers affected by the random external forces. The range II is a part of the sub-ion-scale neighbouring to the MHD-scale, resolved by DNS and LES-H. The range III is also a part of the sub-ion-scale, which is included only DNS. For all the PDFs over the three ranges, the abscissa is normalized by the deviation of each PDF, as J_i/σ_{J_i} where $\sigma_{J_i} = \sqrt{\left\langle J_i^2 \right\rangle - \langle J_i \rangle^2}$ is the deviation of the current components at each scale.

In Fig. 3 (a), the three current density components J_i of DNS and LES-H in the MHD-scale are presented. The solid line represents the Gaussian distribution $P(J_i/\sigma_{J_i}) \propto \exp\left(-(J_i/\sigma_{J_i})^2\right)$. The PDFs collapse to each other. Though the PDFs of LES-L are excluded for clarity of plots, the PDFs collapse with them, too. PDFs of other

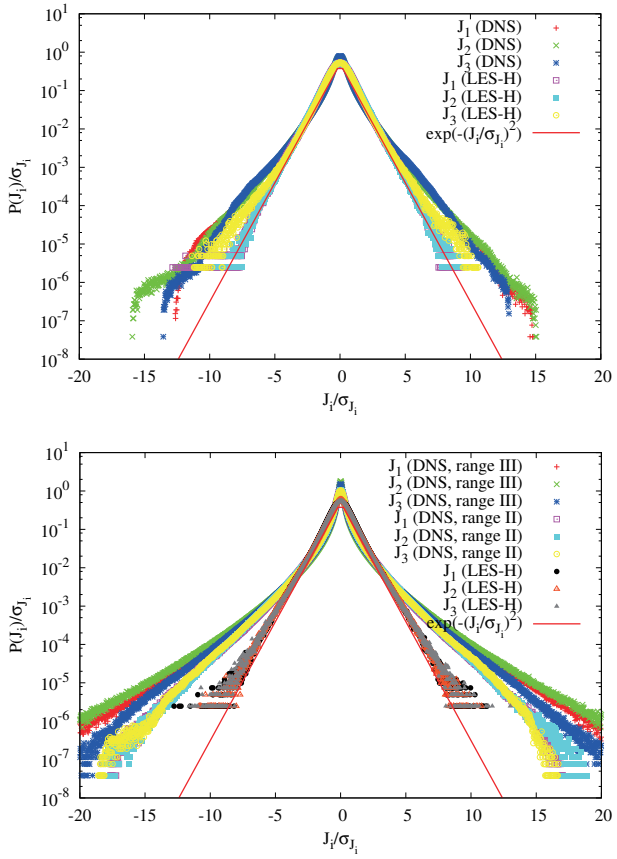

Fig. 3 PDF of the three components of the current density J_i ($i = 1, 2, 3$) in (a) the MHD-scale (range I) and (b) sub-ion-scale (range II).

quantities such as the vorticity components, which are not shown in this paper due to a restriction in page numbers, also collapse among DNS, LES-H, and LES-L as well. In this sense, our LES reproduces the turbulent statistics in MHD-scale well by the use of the SGS model. This is what we expect for LES of Hall MHD turbulence.

In Fig. 3 (b), the PDFs of J_i in the range II and III of DNS, and those in the range II of LES-H and LES-L are presented. The PDFs of J_i of DNS in the two ranges II and III do not collapse to each other. The differences indicate that the intermittency in the sub-ion-scale is stronger in a higher wave-number. The PDFs of J_i of LES-H appear less intermittent than those of DNS. This has been expected because the dynamics of LES-H in this range is fully dominated by the energy sink nature of the SGS model.

It should be emphasized that disagreement between the PDFs of DNS and those of LES-H above is not necessarily a negative result. The essential part of this study is the MHD-scale in the range I, turbulent dynamics of where should be strongly influenced by the sub-ion-scale in the range II neighbouring to I. The stiffness and resolution-demanding nature of the Hall term are successfully suppressed by the SGS model at the expense of the energy sink at this range, as we intend for LES. Thus our intention of LES has been achieved as we have seen in Fig. 3 (a).

Table 2 Ratios of the deviations of the current components in DNS and LES.

	DNS	LES-H	LES-L
$10 < k \leq 20$	1.6	1.1	1.1
$20 < k \leq 40$	1.4	1.0	1.0
$40 < k \leq 80$	1.2	-	-

Here we need to note the normalization of the PDFs by σ_{J_i}. Although the PDFs in Fig. 3 (a) collapse to each other, the raw values of J_i and the normalization by σ_{J_i} can be different between the directions parallel to and perpendicular to the uniform magnetic field B_0 because of the anisotropy of homogeneous turbulence [18–20]. In order to study the difference associated with the normalization, we see $2\sigma_{J_3}/(\sigma_{J_1} + \sigma_{J_2})$. This quantity represents the ratio of the deviation of the current density components in the parallel direction to that in the perpendicular direction. We expect that this quantity represents an aspect of the spectral anisotropy. While J_3 consists of only B_1 and B_2 (perpendicular components), J_1 and J_2 consists of both the parallel (B_3) and perpendicular (either B_1 or B_2) magnetic field component. Thus the spectral anisotropy can induce the difference between J_3 and the other two components.

The ratio of the deviations is presented in Table 2 at three wave-number ranges I-III. In DNS, the ratio becomes larger for smaller wave-number ranges, indicating that the spectral anisotropy is clearer in the MHD-scale than that in the sub-ion-scale. In other words, the Hall term works in this simulation to suppress the anisotropy at the small scale. On the contrary, in the two LES, the ratio stays almost unity whether it is in the MHD-scale or the sub-ion-scale. If a locally strengthened dissipation of the SGS suppresses the difference of the deviation, this result suggests that the sub-ion-scale (or the dissipation scale in single-fluid MHD turbulence as well) plays a crucial role in forming the spectral anisotropy. By updating the SGS model and studying this ratio, we can study the physics of the anisotropy by LES with a smaller computational cost than by DNS.

4. Concluding Remarks

We have carried out DNS and LES of homogeneous Hall MHD turbulence. We have shown that our SGS model developed in Ref. [13] reproduces magnetic and kinetic energy spectra in the perpendicular and parallel direction as well as the PDF of the current density components in the MHD-scale. This enables us to study Hall MHD turbulence and turbulence-related phenomena such as short-wavelength ballooning instability in torus plasma by means of LES with a higher effective resolution than the previous model [11].

In this numerical work, the energy level of the magnetic energy spectrum in the parallel direction of LES is higher than that of DNS at the moderate wave-number

range. Although we do not have a clear explanation, this difference may be related to a strong coupling between distant Fourier wave-numbers by the Hall term [9] and the spectral anisotropy which has been reported and studied extensively in earlier studies [18–20]. The truncation of high wave-number Fourier coefficients by a low-pass filter in LES can induce a large change in the magnetic energy transfer function even at a low wave-number [9]. Though our SGS model is provided in order to compensate for such a role of high wave-number coefficients phenomenologically, the strength of the nonlinear coupling is modified by the uniform magnetic field in this paper. Consequently, the magnetic energy transfer among the scales is lowered, and the magnetic energy stagnates at a moderate wave-number range in LES as we have seen in Fig. 2. This understanding remains conjecture in this paper and is to be studied further in our future work.

We have also found that the anisotropy in the PDFs of the current density can be observed in DNS, especially in its MHD-scale, but not in LES. Since the SGS model works especially in the sub-ion-scale in our simulations, this result suggests that the sub-ion-scale (or the dissipation scale if we study single-fluid MHD turbulence) can play a crucial role in forming the spectral anisotropy. We should study the physics of the anisotropy with a smaller computational cost by LES than by DNS by updating our SGS model in our future work, too.

This research was supported partially by JSPS KAKENHI Grant Number 20H00225, Japan, and partially by the NINS program of Promoting Research by Networking among Institutions. The numerical simulations were performed on NEC SX-Aurora TSUBASA A412-8 *Plasma Simulator* of National Institute of Fusion Science (NIFS), Japan, with the support and under the auspices of the NIFS Collaboration Research program (NIFS22KISS007, NIFS20KNSS133, NIFS20KNTS063), as well as on the FUJITSU FX1000 *Wisteria/BDEC-01 Odyssey* of the University of Tokyo, being partially supported by "Joint Usage/Research Center for Interdisciplinary Large-scale Information Infrastructures" (Project ID: jh220005) and the HPCI System Research Project (Project ID: [redacted]) in Japan.

[1] P.S. Iroshnikov, Sov. Astron. **7**, 566 (1964).
[2] R.H. Kraichnan, Phys. Fluids **8**, 1385 (1965).
[3] P. Goldreich and S. Sridhar, ApJ **435**, 680 (1997).
[4] W.H. Matthaeus *et al.*, Geophys. Res. Lett. **30**, GL017949 (2003).
[5] P. Mininni, A. Alexakis and A. Pouquet, J. Plasma Phys. **73**, 377 (2007).
[6] S. Galtier, Phys. Rev. E **77**, 015302 (2008).
[7] D. Hori and H. Miura, Plasma Fusion Res. **3**, S1053 (2008).
[8] R. Meyrand and S. Galtier, Phys. Rev. Lett. **109**, 194501 (2012).
[9] H. Miura and K. Araki, Plasma Phys. Control. Fusion **55**, 014012 (2013).
[10] H. Miura and K. Araki, Phys. Plasmas **21**, 072313 (2014).
[11] H. Miura, K. Araki and F. Hamba, J. Comput. Phys. **316**, 385 (2016).
[12] H. Miura, F. Hamba and A. Ito, Nucl. Fusion **57**, 076034 (2017).
[13] H. Miura and F. Hamba, J. Comput. Phys. **448**, 110692 (2022).
[14] D. Pekurovsky, SIAM J. Sci. Comput. **34**, C192 (2012).
[15] D. Takahashi, http://www.ffte.jp/ (2014); D. Takahashi, Fast Fourier Transform Algorithms for Parallel Computers, Springer Nature Singapore Pre Ltd. (2019).
[16] F. Hamba and M. Tsuchiya, Phys. Plasmas **17**, 012301 (2010).
[17] A. Yoshizawa and N. Yokoi, Phys. Plasmas **5**, 2902 (1998).
[18] W.H. Matthaeus *et al.*, J. Geophys. Res. **101**, 7619 (1996).
[19] L. Yang *et al.*, ApJ **920**, 14 (2021).
[20] J. Zhang *et al.*, ApJ **924**, L21 (2022).